New compounds and structures in the solid state

Edmund J. Cussen
DOI: 10.1039/b818290f

This Chapter reviews the 2008 literature on new compounds and structures in the solid state.

Highlights

The outstanding highlights from the literature on solid state compounds have arisen from work on a series of compounds that were not widely studied prior to 2008. The observation of superconductivity in a series of iron arsenic compounds spurred a huge research effort that lead to a rapid identification of a number of closely related superconducting phases. These high temperature superconductors show transition temperatures that are higher than any other non-cuprate materials and research in this area is sure to continue vigorously. Other outstanding reports include structures of considerable complexity. A study of the (Ba,Ca,Nd)$FeO_{3-\delta}$ system showed that it is possible to combine structural motifs from a number of different cation- and vacancy-ordered perovskites into a single, complex crystal structure. Whilst the perovskite structure has previously shown a range of subtle structural effects it is surprising that an even more complex structure should arise from the characterisation of the structural properties of an element. A study of the room temperature melting behaviour of sodium under applied pressure has led to the identification of no fewer than six new allotropes of this element. Five of these structures have not previously been observed for any element and some display remarkable complexity with unit cells volumes of up to *ca.* 4918 $Å^3$.

1. Oxides

The perovskite structure continues to be a source of interesting new compounds and even in relatively simple stoichiometries can show new behaviour. Complex spin and orbital ordering is a feature of the perovskite YVO_3 and the origins of these effects have been investigated by studying the mixed V^{3+}/V^{4+} phase $Y_{0.6}Cd_{0.4}VO_3$ that can be prepared under elevated pressure.[1] This compound adopts the common $GdFeO_3$ distorted variant of the simple cubic perovskite structure between room temperature and 2 K. However, the lattice parameters and the VO_6 octahedra both show anomalies around 150 K indicative of a phase change occurring at this temperature. These structural effects are accompanied by features in both the magnetic susceptibility and the specific heat. The broad nature of this structural transition, and the extension in two of the six vanadium-oxide bond lengths, suggest that orbital correlations are involved in a complex transition that has no obvious analogues in

WestCHEM, Department of Pure and Applied Chemistry, The University of Strathclyde, Glasgow, Scotland, UK G12 8PT. E-mail: Edmund.Cussen@Strath.ac.uk; Fax: +44 141 548 4822; Tel: +44 141 548 2797

This journal is © The Royal Society of Chemistry 2009

the YVO_3 parent phase. The compound Ba_2SmMoO_6 has been reported previously, but a neutron diffraction study has provided a more detailed structural picture that reveals a previously undetected distortion and exceptional magnetic behaviour. The charge and size differences between the Sm^{3+} and Mo^{5+} cations leads to ordering of these species in a rock salt pattern across the octahedrally-coordinated sites of the perovskite structure. By preparing samples using ^{154}Sm the problems of neutron absorption due to ^{149}Sm that dominate any scattering experiments using natural abundance samarium can be avoided. This approach has revealed that Ba_2SmMoO_6 undergoes a structural distortion from $I4/m$ to $I\bar{1}$ on cooling below 353 K that leads to negative thermal expansion in the direction of the pseudo-tetragonal distortion. This compound undergoes an antiferromagnetic ordering transition at 130 K that is accompanied by a further structural distortion driven by a Jahn–Teller distortion of the MoO_6 octahedra. This partially lifts the pseudo triple degeneracy associated with t_{2g} ground state of the Mo^{5+} cation.[2]

Whilst these relatively simple stoichiometries can afford complex electronic behaviour it should be noted that the perovskite can accommodate a wide range of ordering schemes of both cations and anions and vacancies on either or both of these ion subsystems. An indication of the potential for complexity, and some of the methods that are necessary to control it, are illustrated by an extensive survey of the structural properties of compounds in the (Ba, Ca, Nd)$FeO_{3-\delta}$ system.[3] This series of compounds was studied in order to combine the different structural features observed in the $NdBaFe_2O_{5+\delta}$ and $Ca_2Fe_2O_5$ members of the series. The former contains iron in FeO_5 square-based pyramidal coordination, whilst the latter contains an ordered arrangement of FeO_4 tetrahedra and FeO_6 octahedra. Careful examination of the oxides with a 2:2:2:6 ratio of Ca:Ba:Nd:Fe found that extensive ordering of both the cations and anion vacancies could be manipulated to give control of the iron environments in a series of compounds. The most reduced phase, $Ca_2Ba_2Nd_2Fe_6O_{15.6}$, involved a 20-fold increase in the size of the unit cell compared to the primitive perovskite substructure and contains iron in octahedral, square pyramidal and trigonal planar coordination environments and an ordered arrangement of the Ca^{2+}, Ba^{2+} and Nd^{3+} cations across eight, ten and twelve coordinate sites in a structure. This structure can be considered as an intergrowth of the $Ca_2Fe_2O_5$ and $YBa_2Fe_3O_8$ structures.

An additional feature of the perovskite structure that can provide even further structural diversity is the ability to combine face-sharing and corner-sharing of oxide octahedra in a range of hexagonal perovskites. An alternating arrangement of corner- and face-sharing leads to a four layer periodic repeating hexagonal structure, as is well-known in a number of manganates including $Ba_{0.5}Sr_{0.5}MnO_{3-\delta}$. These compounds can be reduced further by reaction with LiH or NaH in the temperature range $150 \leq T/^{\circ}C \leq 350$ to remove oxide ions up to a limit of $\delta = 1$.[4] This introduction of a large number of oxide vacancies results in the replacement of the three-dimensionally network of MnO_6 octahedra with isolated Mn_2O_6 units composed of edge-sharing tetrahedrally-coordinated MnO_4 units as shown in Fig. 1. Despite this disruption of the connectivity in the magnetic sublattice $Ba_{0.5}Sr_{0.5}MnO_2$ orders antiferromagnetically, with a canted spin arrangement at the surprisingly high temperature of 355 K suggesting that the formation of such reduced Mn^{2+} phases may be a useful route to materials that are magnetically-ordered under ambient conditions.

A slightly more complex arrangement of edge- and corner-sharing of octahedra leads to the five layered repeat unit of $BaMn_{0.2}Co_{0.8}O_{2.80}$.[5] The ordering of the oxide

This journal is © The Royal Society of Chemistry 2009

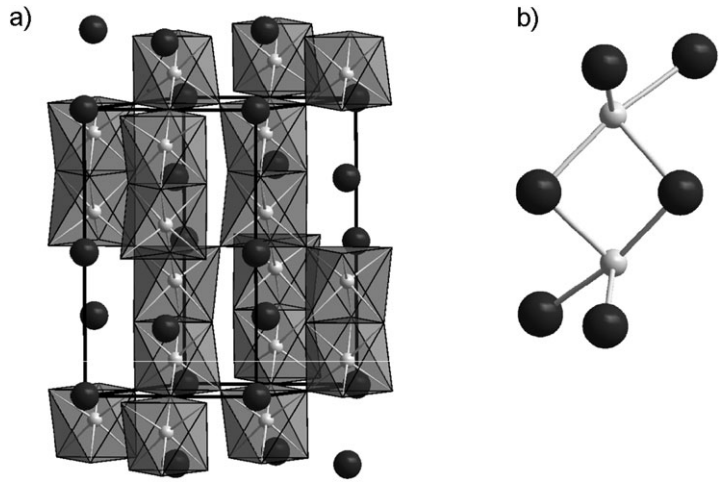

Fig. 1 The 4H structure of $Ba_{0.5}Sr_{0.5}MnO_3$ shown in (a) can be reduced to give $Ba_{0.5}Sr_{0.5}MnO_2$. The face-sharing linkages between the octahedra in the 4H structure are disrupted to give edge-sharing between MnO_4 tetrahedra in $Ba_{0.5}Sr_{0.5}MnO_2$ shown in (b). Light and dark grey spheres represent Mn^{2+} and oxide anions, respectively.[4]

vacancies in this compound again leads to the disruption of the three-dimensional connectivity, in this case discrete blocks of three face sharing octahedra of composition $MnCo_2O_{12}$ are linked *via* shared corners to terminal CoO_4 tetrahedra. The octahedra are occupied by a mixture of Co^{3+}, Co^{4+} and Mn^{4+} whilst the tetrahedra are occupied exclusively by Co^{4+}. This compound is isostructural with the manganese-free analogue $BaCoO_{2.80}$ but shows more complex magnetic behaviour. Although the high temperature, paramagnetic regime indicates ferromagnetic coupling, the material does not display long-range magnetic order but instead forms ferromagnetic clusters below 35 K.

A series of layered perovskite analogues have been reported with the compositions $Pr_{3-x}Sr_{1+x}CrNiO_8$ $0.1 \leq x \leq 1.0$.[6] These compounds contain a mixture of chromium and nickel on the octahedrally-coordinated positions in the perovskite layer that is separated by a mixture of Pr^{3+} and Sr^{2+} cations. These compositions were selected in order to favour the formation of a ferromagnetically-coupled magnetic ground state as predicted for the interaction between the $Ni^{2+}(d^8)$ and $Cr^{3+}(d^3)$ cations. The presence of different cations in the interlayer region was designed to stabilise an ordered arrangement of the transition metal cations in the perovskite layer. However, the small difference in charge and size between Ni^{2+} and Cr^{3+} is insufficient to drive the formation of a cation ordered array and so complex magnetic properties arise from a mixture of competing ferromagnetic and antiferromagnetic superexchange interactions. These lead to the formation of a spin glass phase below a magnetic transition that decreases in temperature from 52 K to 13 K as the strontium content is increased. A complex distribution of cations is also observed in the new Aurivillius phase $Bi_2SrNa_2Nb_4O_{15}$.[7] As in the $Pr_{3-x}Sr_{1+x}CrNiO_8$ system this compound contains slabs of the perovskite structure, in this case composed of four layers of NbO_6 octahedra separated by a layer of Bi_2O_2. The perovskite slab contains an unusual mixture of Sr^{2+}, Na^+ and Bi^{3+} cations and the distribution of charge in these cations is partly compensated by displacements of the Nb^{5+} cations on the edge of the perovskite block away from the

This journal is © The Royal Society of Chemistry 2009

centre of the oxide octahedron. Treatment of this compound with HCl affords almost complete exchange of the interlayer $[Bi_2O_2]^{2+}$ with protons to give a solid acid with the composition $H_{1.8}[Bi_{0.2}Sr_{0.8}Na_2Nb_4O_{13}]$. A similar acid treatment has been used on the triple layered perovskite material $KCa_2Nb_3O_{10}$ to give the solid acid $HCa_2Nb_3O_{10} \cdot 0.3H_2O$.[8] This compound was reacted with tetramethylammonium hydroxide to give exfoliated nanosheets that could be assembled into a crystalline phase $KCa_2Nb_3O_{10} \cdot 1.3H_2O$ by treating with aqueous KCl. These reactions show that the perovskite layer remains intact throughout a number of reactions, and can be used to form metastable hydrated phases that cannot be prepared through conventional high temperature reaction processes.

The perovskite structure is also adopted by a number of multiferroic compounds, *i.e.* materials that display both bulk magnetic and electric dipoles. The compound $La_{0.5}Bi_{0.5}Mn_{0.5}Fe_{0.5}O_{3.09}$ contains a disordered arrangement of La^{3+}/Bi^{3+} and Mn^{3+}/Fe^{3+} on the twelve- and six-coordinate sites of the perovskite structure, respectively. This absence of cation ordering, combined with a tilting of the oxide octahedra leads to this compound adopting the $GdFeO_3$ structure in the space group Pnma. This material undergoes a ferromagnetic ordering transition on cooling below 240 K, presumed to arise from the ferromagnetic coupling between Fe^{3+} and Mn^{3+} dominating over the antiferromagnetic interaction between like cation pairs. This material also shows a remnant polarisation below 67 K that can be switched by application of an electric field and it is argued that despite the random distribution of Bi^{3+} cations in the structure, the sterically-active lone pair of electrons on this species induce the local distortions that cause this effect.[9] A doping study of the rhombohedral multiferroic phase $BiFeO_3$ has shown that room temperature ferromagnetic ordering persists in the series $Bi_{1-x}Pb_xFe_{1-x}Ti_xO_3$ as long as the *R*3*c* space group symmetry is preserved. As the value of x is increased a tetragonally-distorted phase is formed in which no long-range magnetically ordered moment is observed at room temperature.[10]

The multiferroic material $YMnO_3$ does not adopt the perovskite structure as might be anticipated, but instead contains a layered arrangement of corner sharing trigonal bipyramidally-coordinated Mn^{3+} cations. On cooling, this material undergoes a large structural rearrangement without lowering the symmetry from the $P6_3cm$ space group observed in the paramagnetic room temperature structure. At the antiferromagnetic transition temperature every atom in the structure undergoes an exceptionally large displacement in the range 0.05 to 0.09 Å. This giant magneto-elastic effect gives rise to strong coupling between the ferroelectric polarisation and the antiferromagnetic ordering observed in this compound and so is the key to realising multiferroic behaviour in these compounds in the absence of orbital degrees of freedom, and Jahn–Teller activity, that would be afforded by an octahedral coordination environment for Mn^{3+} in the perovskite structure.[11]

The second order Jahn–Teller effect has been exploited in a series of compounds based on d^0 cations. $KNbW_2O_9$, $RbNbW_2O_9$ and $KTaW_2O_9$ are all polar, noncentrosymmetric tungsten bronze compounds. The d^0 configurations of Nb^{5+}, Ta^{5+} and W^{6+} lead to large displacements in the cation position from the centre of the oxide octahedra of up to 0.16 Å and the ferroelectric ordering of the resultant dipoles gives access to a range of useful properties including second harmonic generation, piezoelectricity and pyroelectricity although partial cancellation of the local polarisations leads to relatively small responses.[12] Similar effects have been exploited in the new compound $ZnSnO_3$ to generate a new polar material with the $LiNbO_3$ structure. $ZnSnO_3$ is synthesised under high pressure and, once the sample

This journal is © The Royal Society of Chemistry 2009

has been quenched to ambient conditions, contains Zn^{2+} in a substantially under-bonded coordination environment. Whilst both the Sn^{4+} and Zn^{2+} cations occupy oxide octahedra, the Zn^{2+} cation is substantially displaced towards three of the oxide anions and this gives rise to a large polarisation of 59 $\mu C\ cm^{-2}$. This suggests that exploiting the covalency of Zn^{2+} could provide a new route to polar materials.[13]

The layered cobaltates Na_xCoO_2 show a number of useful properties including ion mobility, large thermoelectric power and, when in hydrated form, superconductivity. These compounds contain layers of edge-sharing CoO_6 octahedra with Na^+ cations in the interlayer space. Depending on the stacking of the CoO_6 layers a range of possible Na^+ coordination environments exist. For the observed arrangement of the layers there are two different interstices, one of which is linked to CoO_6 by shared faces whilst the other is linked by shared edges. Despite this substantial difference between the potential cation sites the Na^+ occupies both positions. There is an anomaly in the conductivity of this compound around 160 °C that arises from a redistribution in the cations between these two sites.[14] Above this temperature the structure contains more sodium on the electrostatically unfavourable position and, as the sample is cooled, some of these cations migrate through the interlayer space to the lower energy position. This higher temperature phase shows a large displacement of both sodium cations from the centre of the trigonal prismatic coordination sites. The low temperature arrangement of cations reduces the repulsion between the cations and leads to a substantially reduced cation displacement.

The cation-ordered phases Li_2MO_3 (M = Ir, Pt) contain a similar layering of cations, but the departure of Li:M from an equimolar ratio cannot be accommodated by a strict alternation between sheets composed of LiO_6 and MO_6 octahedra. Instead the alternating layers are occupied by either Li^+ or else a mixture of Li and M. The mixed cation layers contain an ordered arrangement of Li and M and drive a reduction in symmetry from rhombohedral to monoclinic symmetry. Despite the shared structural features the properties of these two compounds differ substantially, Li_2IrO_3 is metallic but Li_2PtO_3 is a wide bandgap semiconductor.[15]

A careful examination of the structure of the battery material Li_2FeSiO_4 has shown that previous descriptions of this compound had underestimated the symmetry. This material contains Fe^{2+} and Si^{4+} in oxide tetrahedra that are substantially distorted to a trigonal pyramidal geometry. These units are linked to one another by shared vertices to give one-dimensional linkages with a strict alternation between FeO_4 and SiO_4 units.[16] The orientation of these units alternates in a paired arrangement that leads to an expansion of the previously proposed structural model and a reduction in space group symmetry to $P2_1$.

The high mobility of lithium in the garnet structure has led to the study of a number of new compounds in the search for potential solid state lithium electrolytes. Garnets conventionally have a 3:3:2 ratio of cations that occupy square antiprismatically-, tetrahedrally- and octahedrally-coordinated positions as demonstrated in $Na_3Ga_3Te_2O_{12}$.[17] A number of cation-rich lithium-containing garnets have been reported which show fast lithium conduction at room temperature. The phases $Li_6ALa_2Nb_5O_{12}$ (A = Ca, Sr) contain lithium cations on a mixture of the tetrahedral sites conventionally occupied in the garnet structure and additional oxide octahedra that are usually unoccupied in garnets. These compounds show a lithium conductivity of *ca.* 10^{-6} S cm^{-1} at room temperature. It was noted that quenching the sample from 700 °C stabilised a slight increase in the lithium occupation of the oxide octahedra and a reduction in the tetrahedrally-coordinated position. This was associated with an increase in the total conductivity of the sample.

This journal is © The Royal Society of Chemistry 2009

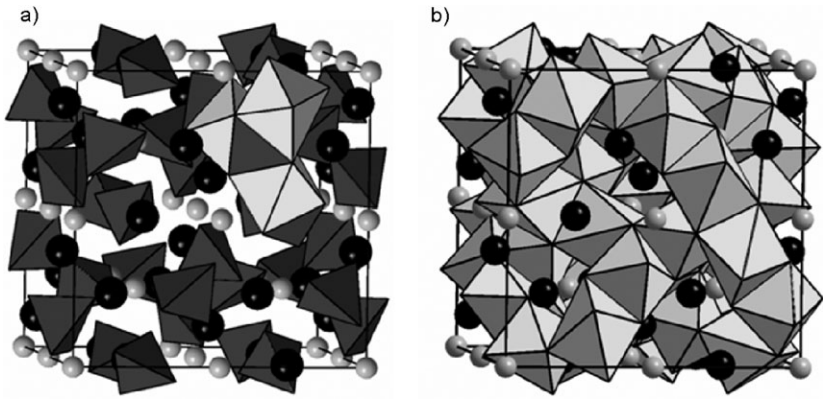

Fig. 2 The lithium rich garnets contain lithium in a mixture of oxide tetrahedra and octahedra shown as dark and light polyhedra, respectively in (a). The pathway for fast lithium conduction in $Li_{3+x}Nd_3Te_{2-x}Sb_xO_{12}$ is formed from the edge sharing network of octahedra shown in (b). Black and light grey spheres represent neodymium and tellurium/antimony, respectively.[19]

The activation energy for the process remains largely unchanged suggesting that the enhancement in lithium conduction arises from a change in carrier concentration rather than a different process, or a change in microstructure of the sample.[18] The garnet phases from the $Li_{3+x}Nd_3Te_{2-x}Sb_xO_{12}$ system have been studied in detail using a combination of X-ray and neutron diffraction, solid state NMR and impedance spectroscopy measurements.[19] This combination of techniques has been bought to bear on the interface between the highly-conducting, lithium-rich phases, such as $Li_4Nd_3TeSbO_{12}$, and the conventional garnet stoichiometries, such as $Li_3Nd_3Te_2O_{12}$, that show only limited lithium mobility at high temperature and undetectable mobility at room temperature. This showed that the lithium distribution across the oxide tetrahedra and distorted octahedra evolves smoothly as the lithium content of the garnet is increased. The conductivity of these compounds undergoes a step change on increasing the lithium content beyond the conventional stoichiometry, with a change in activation energy from 1.3 eV for $Li_3Nd_3Te_2O_{12}$ to 0.67 eV for $Li_{3.05}Nd_3Te_{1.95}Sb_{0.05}O_{12}$. As NMR shows that the behaviour of lithium in the LiO_4 units is the same in both compositions these measurements show that the fast lithium conductivity in garnets arises from lithium mobility through the three-dimensional network composed of edge sharing oxide-octahedra shown in Fig. 2. This distribution of lithium across two different polyhedra is a consistent feature of these lithium-rich compounds.[20,21]

2. Halides and oxyhalides

The most dramatic development in solid state chemistry in 2008 came from the properties of a family of compounds related to the layered iron compound LaOFeAs. This compound contains iron atoms tetrahedrally coordinated by four arsenic atoms and these $FeAs_4$ units are linked *via* shared edges to give sheets that are separated from one another by layers of LaO as shown in Fig. 3. The interest in this structural family was stimulated by the report that electronically doping the system, by replacing some of the oxide anions with fluoride, gave compounds $LaO_{1-x}F_xFeAs$ which for compositions in the range $0.04 \leq x \leq 0.12$ show superconductivity at temperatures up to 26 K.[22] This unexpected observation

This journal is © The Royal Society of Chemistry 2009

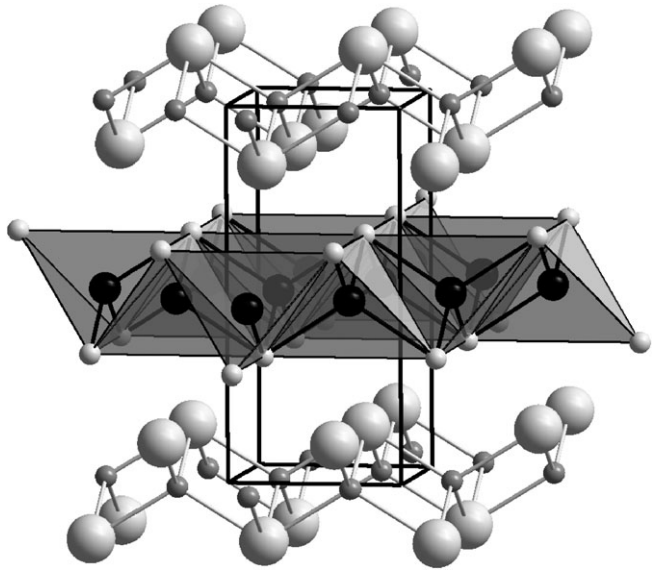

Fig. 3 The crystal structure of LaOFeAs contains a layer of edge sharing $FeAs_4$ represented as grey tetrahedra. The lanthanum and oxygen atoms are shown as large and small grey spheres, respectively.[22]

provoked a flurry of activity that quickly established that the superconducting state persisted at exceptionally high field[23] and exists in a compositionally wide-ranging family. Replacement of La^{3+} with Sm^{3+} gave the series $SmO_{1-x}F_xFeAs$ and for the $x = 0.15$ composition a dramatic increase in the superconducting transition temperature to 43 K, at the time the highest T_C for any non-cuprate material. This also demonstrated that in common with the cuprates, the superconductivity in these iron arsenides cannot be explained by BCS theory.[24]

A number of different compounds with Nd, Pr, Sm and Gd have since been reported where the transition temperature has increased to above 50 K.[25–27] A study of the superconducting phase $NdFeAsO_{0.80}F_{0.20}$ showed similar structural features to the La^{3+} analogues and the authors concluded that the doubling in T_C that occurs on replacement of La^{3+} with Nd^{3+} is substantially due to the smaller size of Nd^{3+} rather than more complex effects.[28] The over-riding importance of the FeAs layers is clearly demonstrated by the observation of superconductivity in a series, $K_{1-x}Sr_xFe_2As_2$, that uses metals rather than a lanthanide oxide to dope the FeAs layer. The T_C of the $K_{1-x}Sr_xFe_2As_x$ series varies rapidly with composition. The observations of similar properties in the caesium analogue[29] and in $K_{0.4}Ba_{0.6}Fe_2As_2$ indicate[30,31] the dominant effect of the FeAs layers on the electronic properties of this new family of superconductors.

Unusual physical properties have also been reported in a number of reduced dimensional halides. Solvothermal treatment of InF_3 or ScF_3 in the presence of 1,3-diaminobutane has led to the formation of the new compounds $[C_4H_{14}N_2][MF_5]$ containing chains of MF_6 octahedral units linked *via* shared vertices in a *trans* arrangement to give linear chains of $(MF_5)_\infty$. These compounds can be doped with either Eu^{3+} or Tb^{3+} cations to give orange or green photoluminescence, respectively. Whilst the small quantities of lanthanide cation could not be located crystallographically these cations are presumably incorporated in place of the In^{3+}

This journal is © The Royal Society of Chemistry 2009

or Sc^{3+} cations. An interesting consequence of this incorporation is that the luminescence of a sample co-doped with both lanthanides shows that the emission of Eu^{3+} is enhanced by the presence of Tb^{3+} within the same lattice.[32]

The strongly two-dimensional structure of $Cu_3Zn(OH)_6Cl_2$ provides a strong model for a geometrically-frustrated Kagome lattice. The structure of this compound contains an ordered arrangement of paramagnetic Cu^{2+} and diamagnetic Zn^{2+} over the sites of a pyrochlore-like lattice. In the absence of chemical ordering, these cations would form a triangular array but in this new metastable polymorph the complete cation ordering introduces diamagnetic holes into the paramagnetic net and produces a Kagome net populated by the $S = 1/2$ Cu^{2+} cation. Interlayer magnetic interactions appear to be weak and preliminary magnetic measurements suggest that these spins may be condensing to the desired nonmagnetic ground state.[33]

Hydrothermal syntheses have produced a range of compounds $Ln_2(OH)_5X \cdot 1.5H_2O$ where Ln = Y, Dy, Er and Yb and X = Cl or Br. These compounds are the first examples of a new family of doped, layered-hydroxides that follow the formula $Ln_2(OH)_{6-y}X_y$. The Yb^{3+} composition yields two polymorphs that both crystallise in noncentrosymmetric space groups. All other lanthanides afford a single polymorph that contains the Ln^{3+} cation in a mixture of seven- and eight-coordinate positions to form positively charge layers. This charge is balanced by halide anions that occupy the interlayer space. These anions can be readily exchanged by reaction with dicarboxylic acid salts and, in the case of $Er_2(OH)_5Cl \cdot 1.5H_2O$, complete exchange can be achieved at room temperature with a wide range of dicarboxylate anions.[34]

An alternative method of exchanging anions is demonstrated in the synthesis of a new oxide fluoride $Ba_2SnO_{2.5}F_3 \cdot xH_2O$, $x \approx 0.5$.[35] The layered perovskite analogue Ba_2SnO_4 was prepared using conventional high temperature methods and then reacted with a fluorinating agent, ZnF_2 at the relatively low temperature of 240 °C. The tetragonal space group symmetry of the Ba_2SnO_4 parent is preserved in the resulting oxide fluoride albeit with a large increase in the c lattice parameter from 13.309 Å to 16.330 Å indicating a considerable increase in the spacing between the perovskite blocks. This increase in interlayer volume is driven by the insertion of both interstitial fluoride and water between the layers. The latter can be removed by heating the sample to afford the dehydrated phase $Ba_2SnO_{2.5}F_3$. A more protracted multi-step synthesis has been used in the preparation of the new oxide fluoride $Sr_7Mn_4O_{13}F_2$.[36] This involved preparing the $Sr_7Mn_4O_{15}$ precursor using a high temperature treatment in air to afford the Mn^{4+} oxidation state. This compound was then reduced using CaH_2 to the Mn^{3+} compound $Sr_7Mn_4O_{13}$ which was then oxidised using 5% F_2 in N_2 to give the new compound $Sr_7Mn_4O_{13}F_2$ with a mean oxidation state of $Mn^{3.5+}$. This sequential reduction and oxidation is carried out at relatively low temperatures and so provides an excellent method to manipulate the anion sublattice and prepare metastable materials. A key result is that, even though the temperature of this process is above that of the initial reduction and so suggests that the oxide anions may not be kinetically trapped in this configuration, the oxidation with fluorine occurs topotactically. Thus the product of this multistep reaction is a structure that contains an arrangement of anions that is unlikely to be achievable in a single-step, high-temperature synthesis.

An even more elaborate synthetic approach has been used in the search for a new polymorph of lithium bromide that has been predicted to be only slightly higher in energy than the usual rock salt structure.[37] By exposing a substrate at −50 °C to a

This journal is © The Royal Society of Chemistry 2009

low vapour pressure of LiBr a new polymorph, β-LiBr, was formed. On warming to room temperature this material transforms to the rock salt structure. The new metastable phase can be grown as a thick layer on either sapphire (001), lithium niobate (001) or polycrystalline copper substrate. X-Ray powder diffraction data show that this is the first experimental evidence for the formation of lithium bromide with the wurtzite structure. This synthetic approach provides a general route to stabilise new structures that lie energetically close to the thermodynamic ground state.

3. Nitrides and chalcogenides

Nitrides and oxynitrides can often be prepared by ammonolysis of an oxide precursor. This relatively simple synthesis has been used in the preparation of the Eu^{2+} phases $EuNbO_2N$ and $EuTaO_2N$. These isostructural compounds adopt the perovskite structure with a slight tetragonal distortion that may arise from a N^{3-}/O^{2-} ordering that is fundamentally undetectable in the X-ray diffraction experiments. Both compounds are electronically insulating and order ferromagnetically around 5 K. Above this temperature the paramagnetic response is that which would be expected for almost completely uncoupled Eu^{2+} magnetic moments. Large negative magnetoresistance is observed in both compounds as the samples are cooled towards the magnetic transition. Below the transition the change in resistivity is reduced by over two orders of magnitude by the application of a field of ≈ 2 T and so earns these compounds the appellation of colossal magnetoresistive materials. This effect is accompanied by a giant positive magnetocapacitance effect of 20% in a field of 4 T at 2 K. The change in charge transport arises from an exchange interaction between the spins of the mobile charge carrying species and the localised moments of the Eu^{2+} cation. However the change in capacitance is not coupled with this effect but is most likely a product of interfacial polarisation arising from grain boundary effects.[38]

Reaction of the simple perovskite $CaMoO_3$ with ammonia has led to the formation of the new oxide-nitride $CaMnO_{1.7}N_{1.3}$. This compound crystallises with the $GdFeO_3$ structure with a random distribution of O^{2-}/N^{3-} over the two crystallographic anion positions. The charge on the anions indicates that the mean oxidation state of molybdenum in this compound should be $Mo^{5.3+}$ although the Mo–O/N bond lengths suggest a lower oxidation state.[39] It is unclear what the impact of this oxidation of molybdenum has on the properties of this perovskite compared to the metallic phase $CaMoO_3$. Attempts to prepare a Ba^{2+} analogue failed to produce the desired product.

A combination of calculations and high pressure synthesis have been used to evaluate the stability of highly condensed calcium nitridosilicate, $Ca_2Si_5N_8$. This phase is formed by heating at 900 °C under an applied pressure of 6 GPa but can be quenched without transforming back to the ambient-pressure polymorph. The centrosymmetric high pressure phase contains buckled layers composed of corner sharing SiN_4 tetrahedra. These layers are linked by additional SiN_4 tetrahedra with Ca^{2+} found in the interlayer region. Despite strong similarities with the low-pressure, non-centrosymmetric polymorph the formation of the high pressure structure requires significant reconstruction and it is likely that this process introduces an activation energy for the transformation between the low- and high-pressure phases that confers metastability on the high pressure phase under ambient conditions. The photoluminescence of a Eu^{2+} doped sample shows that the

This journal is © The Royal Society of Chemistry 2009

high pressure phase produces a narrower emission band than the ambient pressure polymorph and this material may find application as a phosphor for the emission of warm white light.[40]

A new, air-stable layered oxysulfide, $Ba_2Mn_2O_4Cu_{0.9}S$, has been prepared by reaction of a mixture of oxides, sulfides and elemental copper with CS_2. This compound contains an unusual arrangement of four layers of square-based pyramidal MnO_5 units that are linked a mixture of corner- and edge-sharing as shown in Fig. 4. These layers are separated by layers of Cu_2S_2 but despite this reduced dimensionality some of the moments of the $Mn^{2.55+}$ cations participate in long-range antiferromagnetic order.[41] The oxyselenide $Ba_2ZnO_2Ag_{23}Se_2$ also contains interleaved sheets of alternating oxide and chalcogenide. In this compound the oxide layer is composed of discreet, linear ZnO_2 units that are unprecedented. Zn^{2+} is commonly found in tetrahedrally-coordinated oxide environments, but in this compound it is forced into an unusual square planar configuration. This ZnO_4 planar unit is heavily distorted with two Zn–O distances of 1.88(1) Å and two at a distance, 2.40(1) Å, that suggests there is no Zn–O bond. This provides a remarkable example of linear coordination around Zn^{2+} that shows strong parallels with the chemistry of the heavier Group 10 cations Hg^{2+} and Cd^{2+}.[42]

Chromium(III) sulfide, Cr_2S_3, contains an ordered arrangement of chromium cations in the octahedrally-coordinated sites between layers composed of edge-sharing CrS_6 octahedra and is ferrimagnetic below 125 K. Fully occupied edge-sharing octahedra also exist in V_2S_3, but the vanadium cations between these

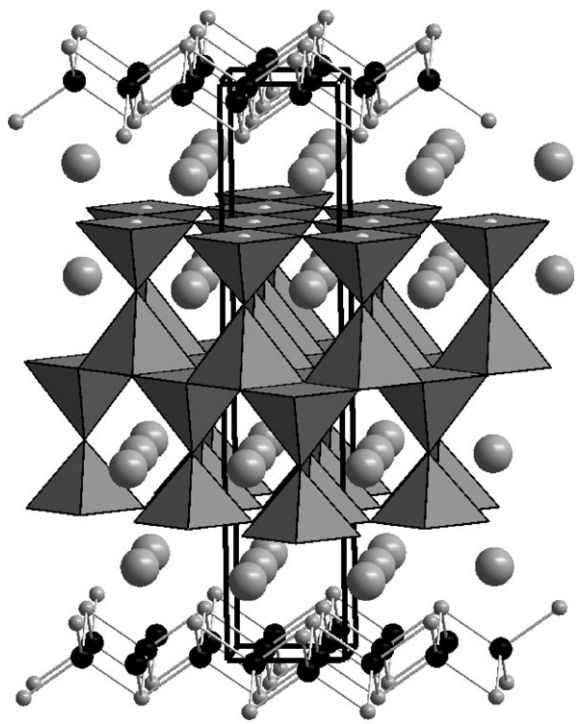

Fig. 4 The structure of $Ba_2Mn_2O_4Cu_{0.9}S$ contains MnO_5 square pyramidal units separated by barium cations, shown as large grey spheres, from a layer of copper sulfide. The copper and sulfur are represented as black and small grey spheres.[41]

This journal is © The Royal Society of Chemistry 2009

layers adopt a different ordering pattern that is similar to that reported in Cr_3S_4. A study of the structural properties of $Cr_{2-x}V_xS_3$ has revealed that vanadium can be introduced into the Cr_2S_3 structure for compositions up to $x = 0.75$ and that chromium can replace vanadium at the other end of the compositional series for $x \geq 1.6$. The replacement of the Cr^{3+}, d^3 cation with the V^{3+}, d^2 cation introduces holes into the t_{2g} manifold and increases the conductivity of the semiconducting Cr_2S_3. As the vanadium content is increased further the conductivity becomes metallic and this is associated with the formation of the cation chains as a consequence of adopting the structure of the V_2S_3 end member.[43]

4. Oxyanions and related phases

Hydrothermal synthesis in a highly concentrated methylamine solution has produced an unusual open framework chalcogenide $[Zn(H_2O)_4][Zn_2Sn_3Se_9(MeNH_2)]$ that crystallises in the space group $P1$. The framework is built from a $[ZnSn_3Se_{10}]^{6-}$ cluster that can most readily be visualised as a tetrahedron composed of four tetrahedra as shown in Fig. 5. These clusters are connected by shared vertices to give chains that are linked in the remaining two-dimensions by Zn_2 linkages to give a negatively charged, three-dimensionally connected framework with a pore volume of 29%. This extra-framework space is occupied by $Zn(H_2O)_4^{2+}$ cations that can be replaced by protons with no significant contraction in the anionic lattice to give the solid acid $H_4[Zn_2Sn_3Se_9(MeNH_2)]$. The polar structure of the as-made material leads to excellent second harmonic generation efficiency that compares favourably with commercial materials.[44]

A new germanosilicate, ITQ-26, has been prepared using 1,3-bis(triethylphosphoniummethyl)benzene dihydroxide as a structure directing agent.[45] The structural analysis of the new phase was a considerable challenge; in addition to containing a impurity phase, the polycrystalline product was poorly ordered and provided Bragg scattering to a *d*-spacing of only 1.8 Å. In order to solve the structure it was necessary to incorporate electron diffraction data in addition to X-ray powder diffraction experiments. The former were analysed using a maximum entropy method to assess the likelihood of the solutions and the structure solution from the diffracted X-ray intensities used a structure recognition algorithm to identify likely connectivity between the tetrahedral subunits. The resultant structure contains

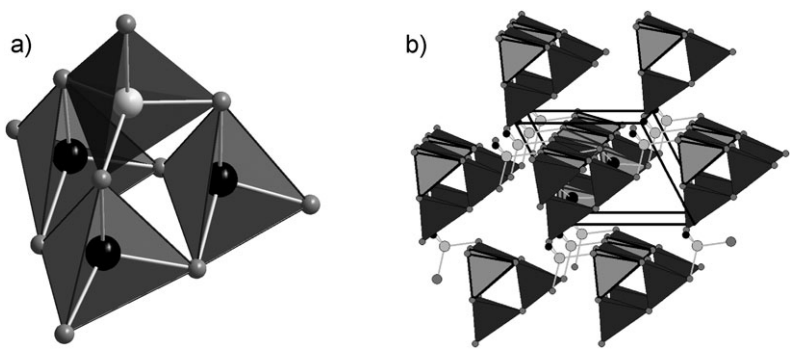

Fig. 5 The framework structure of $[Zn(H_2O)_4][Zn_2Sn_3Se_9(MeNH_2)]$ is built up from tetrahedral units (a) composed of $ZnSe_4$ and $SnSe_4$ represented as grey and black tetrahedra, respectively. These units (b) are linked to form chains along the [100] direction of the unit cell.[44]

This journal is © The Royal Society of Chemistry 2009

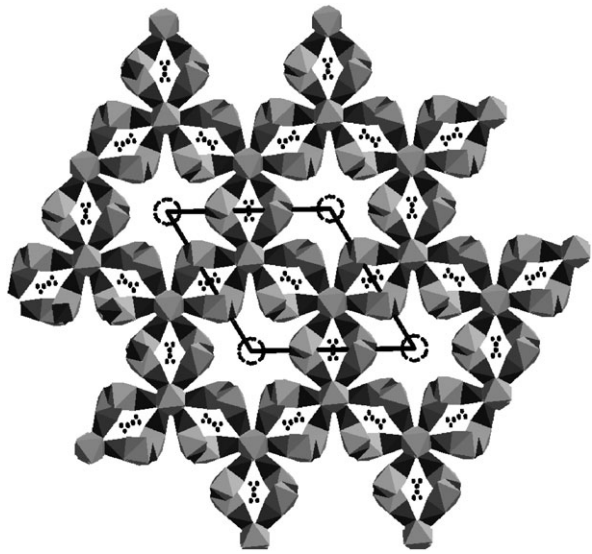

Fig. 6 The structure of $LiTi_2(PS_4)_3$ is composed of an edge-sharing array of TiS_6, shown in grey octahedra, and PS_4 units, shown as black tetrahedra. The Li cations are shown as black spheres.[46]

12-ring channels and a framework density of 14.3 tetrahedral species 1000 $Å^{-3}$ that is lower than other zeolites with a similar channel size. These channels are approximately circular with a diameter of 7 Å and sorption measurements show that once the structure directing agent molecules have been removed from the pores of the as-made material by calcination, this porosity can be accessed by sorption probe molecules.

A new lithium-containing thiophosphate has been prepared using a high temperature solid state reaction.[46] This compound has a relatively open structure formed by a network of edge sharing between TiS_6 octahedra and PS_4 tetrahedra as shown in Fig. 6. These units are linked together to give a honeycomb arrangement of channels that run along the [001] direction of the hexagonal unit cell. The structure contains a large extra-framework volume and an additional seven lithium ions per formula unit can be electrochemically inserted into the material to give a stoichiometry $Li_8Ti_2(PS_4)_3$. This quantity of lithium cannot be achieved purely by reducing Ti^{4+} to Ti^{2+} and it is probable that reduction of $[PS_4]^{3-}$ subunits to $[PS_4]^{4-}$ occurs during the lithium insertion. The material becomes amorphous with repeated cycles of lithium insertion/extraction possibly as a consequence of the redox activity of the thiophosphate ions.

5. Intermetallics

Calculations on the face centred cubic phase of elemental sodium have shown that the longitudinal phonon density of states harden in response to pressure whilst the transverse modes soften and so it has been predicted that the shear modulus of sodium should collapse in response to pressure above 100 GPa. New developments in single crystal experiments have been used to examine the structural behaviour of sodium in this high pressure regime for the first time. The melting temperature of sodium passes through a minimum near room temperature for a pressure of

This journal is © The Royal Society of Chemistry 2009

118 GPa. By varying the pressure within a ±2 GPa range of this minimum six new crystalline phases of elemental sodium have been identified.[47] Five of these have never been observed for any other element. Complete structure solutions have not been realised for all allotropes, but it appears that sodium can demonstrate unprecedented complexity; one of the allotropes adopts a monoclinic structure with a unit cell volume of 4918(2) $Å^3$ that indicates approximately 500 atoms are contained within the unit cell. This is the most complex phase yet observed for any element. The origin of this remarkable abundance of allotropes and astonishing complexity is unclear but it may be related to the quantum effects that have led to the predictions of metallic superfluid behaviour in H_2.

The search for new lanthanide rich oxides has led to the preparation of $La_{10}Si_8O_3$ and $Ce_{10}Si_8O_3$. The lanthanide and oxide species are contained in Ln_6O octahedra that form an array that resembles that of the hexagonal tungsten bronzes based on WO_6 octahedra. This structure contains hexagonal channels and in $Ln_{10}Si_8O_3$ phases these are filled by regular, planar Si_6 units with an inter-silicon distance of 2.38 Å. Electronic structure calculations show that these planar units should be described as $[Si_6]^{6-}$ *i.e.* they are isoelectronic with benzene. Although $[Si_6]^{10-}$ rings have been observed before it appears that the details of the of $Ln_{10}Si_8O_3$ structure destabilise the π* states of the Si_6 ring in the present compounds and so lead to the formation of aromatic $[Si_6]^{6-}$ fragments.[48] Planar hexagons are also a feature of the new superconducting phase $YbGa_{1.1}Si_{0.9}$ although in this compound the sites are occupied by a mixture of gallium and silicon. This material is isostructural with MgB_2 and features Yb^{2+} cations between the regular hexagonal layers of $Ga_{1.1}Si_{0.9}$. This material is a Curie–Weiss paramagnetic above a superconducting transition that occurs at 2.4 K.[49] The Heusler compound $ZrNi_2Ga$ adopts a cubic structure that features an edge-sharing arrangement of ZrNi tetrahedra that is similar to the arrangement of FeAs in the high temperature superconductors based on LaOFeAs.[22] However, the superconductivity in $ZrNi_2Ga$, and the electron

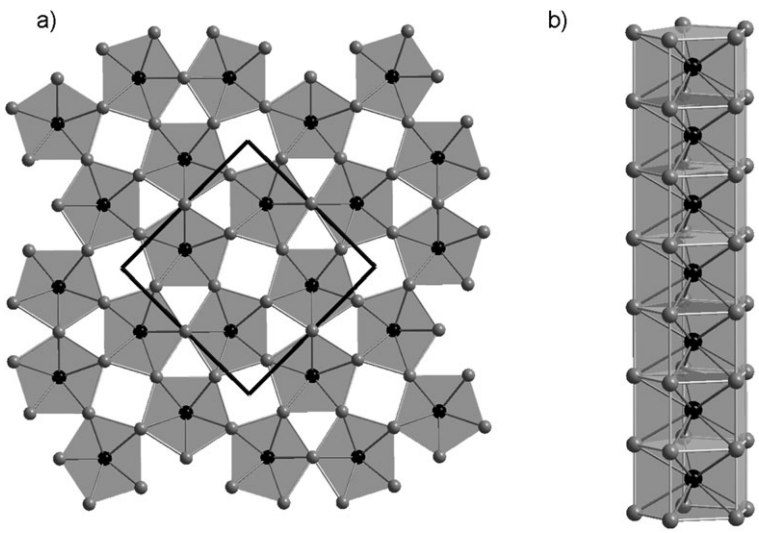

Fig. 7 (a) The structure of Mn_2Ga_5 contains manganese atoms, shown as black spheres, in the centre of pentagonal prism of gallium, shown as grey spheres. These pentagonal prisms form chains (b) that run along the [001] direction of the unit cell.[52]

This journal is © The Royal Society of Chemistry 2009

doped analogues $Zr_{1-x}Nb_xNi_2Ga$, can be understood with reference to conventional BCS theory.[50]

A metastable compound Cd_4Sb_3 has been prepared by quenching from the melt. The simple binary stoichiometry may imply the formation of a relatively simple compound, but the structure crystallises in the monoclinic space group *Pn* with a large unit cell that contains 156 cadmium and 120 antimony atoms. Heating this compound causes a reversible transition to a more disordered structure at 373 K before decomposition to CdSb and elemental cadmium at 520 K. Both the ordered and disordered polytypes of Cd_4Sb_3 show large thermopower approaching 200 $\mu V\ K^{-1}$ at room temperature. Curiously this value is doubled when the material is prepared using elemental tin as a flux, though this may arise from differences between the temperature of the structural analyses and the physical properties measurements.[51] The new binary compound Mn_2Ga_5 also has a simple stoichiometry, but in this case it reflects a relatively simple structure. This structure can be described as a three dimensional network of gallium atoms with all manganese atoms occupying the same crystallographically equivalent position in the centre of a pentagonal prism.[52] As shown in the Fig. 7 the layers in this tetragonal structure bear a resemblance to the arrangement of WO_3 in the hexagonal tungsten bronzes. The $MnGa_{10}$ units are stacked along the *z* direction to give chains of face-sharing pentagons. Below 450 K this compound adopts a ferromagnetic ground state that is stabilised by a large degree of anisotropic degeneracy in the bands that arise from the transition metal d-orbitals.

References

1 A. A. Belik, M. Nagao, M. Azuma, M. Takano, Y. Matsui and E. Takayama-Muromachi, *Chem. Mater*., 2008, **20**, 5246.
2 A. C. Mclaughlin, *Phys. Rev. B*, 2008, 132404.
3 C. Tenailleau, M. Allix, J. B. Claridge, M. Hervieu, M. F. Thomas, J. P. Hirst and M. J. Rosseinsky, *J. Am. Chem. Soc*., 2008, **130**, 7570.
4 J. J. Adkin and M. A. Hayward, *Inorg. Chem*., 2008, **47**, 10959.
5 L. Miranda, A. Feteira, D. C. Sinclair, M. García Hernández, K. Boulahya, M. Hernando, A. Varela, J. M. González-Calbet and M. Parras, *Chem. Mater*., 2008, **20**, 2818.
6 S. E. Dutton, M. Bahout, P. D. Battle, F. Tonus and V. Demange, *J. Solid State Chem*., 2008, **181**, 2217.
7 Z. Liang, K. Tang, S. Zeng, D. Wang, T. Li and H. Zheng, *J. Solid State Chem*., 2008, **181**, 2565.
8 Y. Chen, X. Zhao, H. Mac, S. Ma, G. Huang, Y. Makita, X. Bai and X. Yang, *J. Solid State Chem*., 2008, **181**, 1687.
9 A. K. Kundu, R. Ranjith, B. Kundys, N. Nguyen, V. Caignaert, V. Pralong, W. Prellier and B. Raveau, *Appl. Phys. Lett*., 2008, 93.
10 T. P. Comyn, T. Stevenson, M. Al-Jawad, S. L. Turner, R. I. Smith, W. G. Marshall, A. J. Bell and R. Cywinski, *Appl. Phys. Lett*., 2008, **93**, 232901.
11 S. Lee, A. Pirogov, M. S. Kang, K. H. Jang, M. Yonemura, T. Kamiyama, S. W. Cheong, F. Gozzo, N. Shin, H. Kimura, Y. Noda and J. G. Park, *Nature*, 2008, **451**, 805.
12 H. Y. Chang, T. Sivakumar, K. M. Ok and P. S. Halasyamani, *Inorg. Chem*., 2008, **47**, 8511.
13 Y. Inaguma, M. Yoshida and T. Katsumata, *J. Am. Chem. Soc*., 2008, **130**, 6704.
14 T. Zhou, A. J. Wright, D. Zhang, T. W. Button and C. Greaves, *J. Mater. Chem*., 2008, **18**, 1342.
15 M. J. O'Malley, H. Verweij and P. M. Woodward, *J. Solid State Chem*., 2008, **181**, 1803.
16 S.-i. Nishimura, S. Hayase, R. Kanno, M. Yashima, N. Nakayama and A. Yamada, *J. Am. Chem. Soc*., 2008, **130**, 1312.
17 A. F. Frau, J. H. Kim and P. S. Halasyamani, *Solid State Sci*., 2008, **10**, 1263.
18 J. Percival, D. Apperley and P. R. Slater, *Solid State Ionics*, 2008, **179**, 1693.
19 M. P. O'Callaghan, J. T. Titman, G. Z. Chen and E. J. Cussen, *Chem. Mater*., 2008, **20**, 2360.

This journal is © The Royal Society of Chemistry 2009

20 J. Percival, E. Kendrick and P. R. Slater, *Solid State Ionics*, 2008, **179**, 1666.
21 M. P. O'Callaghan and E. J. Cussen, *Solid State Sci.*, 2008, **10**, 390.
22 Y. Kamihara, T. Watanabe, M. Hirano and H. Hosono, *J. Am. Chem. Soc.*, 2008, **130**, 3296.
23 F. Hunte, J. Jaroszynski, A. Gurevich, D. C. Larbalestier, R. Jin, A. S. Sefat, M. A. McGuire, B. C. Sales, D. K. Christen and D. Mandrus, *Nature*, 2008, **453**, 903.
24 T. Y. Chen, Z. Tesanovic, R. H. Liu, X. H. Chen and C. L. Chien, *Nature*, 2008, **453**, 1224.
25 R. H. Liu, G. Wu, T. Wu, D. F. Fang, H. Chen, S. Y. Li, K. Liu, Y. L. Xie, X. F. Wang, R. L. Yang, L. Ding, C. He, D. L. Feng and X. H. Chen, *Phys. Rev. Lett.*, 2008, 101.
26 Z. A. Ren, J. Yang, W. Lu, W. Yi, G. C. Che, X. L. Dong, L. L. Sun and Z. X. Zhao, *Mater. Res. Innovations*, 2008, **12**, 105.
27 C. Wang, L. J. Li, S. Chi, Z. W. Zhu, Z. Ren, Y. K. Li, Y. T. Wang, X. Lin, Y. K. Luo, S. A. Jiang, X. F. Xu, G. H. Cao and Z. A. Xu, *EPL*, 2008, 83.
28 Y. Qiu, W. Bao, Q. Huang, T. Yildirim, J. M. Simmons, M. A. Green, J. W. Lynn, Y. C. Gasparovic, J. Li, T. Wu, G. Wu and X. H. Chen, *Phys. Rev. Lett.*, 2008, 101.
29 K. Sasmal, B. Lv, B. Lorenz, A. M. Guloy, F. Chen, Y. Y. Xue and C. W. Chu, *Phys. Rev. Lett.*, 2008, **101**, 107007.
30 M. Rotter, M. Tegel and D. Johrendt, *Phys. Rev. Lett.*, 2008, **101**, 107006.
31 A. D. Christianson, E. A. Goremychkin, R. Osborn, S. Rosenkranz, M. D. Lumsden, C. D. Malliakas, I. S. Todorov, H. Claus, D. Y. Chung, M. G. Kanatzidis, R. I. Bewley and T. Guidi, *Nature*, 2008, **456**, 930.
32 A. C. A. Jayasundera, A. A. Finch, P. Wormald and P. Lightfoot, *Chem. Mater.*, 2008, **20**, 6810.
33 R. H. Colman, C. Ritter and A. S. Wills, *Chem. Mater.*, 2008, **20**, 6897.
34 L. Poudret, T. J. Prior, L. J. McIntyre and A. M. Fogg, *Chem. Mater.*, 2008, **20**, 7447.
35 F. J. Berry, E. Moore, M. Mortimer, X. Ren, R. Heap, P. Slater and M. F. Thomas, *J. Solid State Chem.*, 2008, **181**, 2185.
36 I. Saratovsky, M. A. Lockett, N. H. Rees and M. A. Hayward, *Inorg. Chem.*, 2008, **47**, 5212.
37 Y. Liebold-Ribeiro, D. Fischer and M. Jansen, *Angew. Chem., Int. Ed.*, 2008, **47**, 4428.
38 A. B. Jorge, J. Oro-Sole, A. M. Bea, N. Mufti, T. T. M. Palstra, J. A. Rodgers, J. P. Attfield and A. Fuertes, *J. Am. Chem. Soc.*, 2008, **130**, 12572.
39 D. Logvinovich, M. H. Aguirre, J. Hejtmanek, R. Aguiar, S. G. Ebbinghaus, A. Reller and A. Weidenkaff, *J. Solid State Chem.*, 2008, **181**, 2243.
40 S. R. Römer, C. Braun, O. Oeckler, P. J. Schmidt, P. Kroll and W. Schnick, *Chem.–Eur. J.*, 2008, **14**, 7892.
41 G. Hyett, Z. A. Gál, C. F. Smura and S. J. Clarke, *Chem. Mater.*, 2008, **20**, 559.
42 S. J. C. Herkelrath, I. Saratovsky, J. Hadermann and S. J. Clarke, *J. Am. Chem. Soc.*, 2008, **130**, 14426.
43 T. E. Engin, A. V. Powell and S. Hull, *Chem. Mater.*, 2008, **20**, 2039.
44 M. J. Manos, J. I. Jang, J. B. Ketterson and M. G. Kanatzidis, *Chem. Commun.*, 2008, 972.
45 D. L. Dorset, K. G. Strohmaier, C. E. Kliewer, A. Corma, M. J. Díaz-Cabañas, F. Rey and C. J. Gilmore, *Chem. Mater.*, 2008, **20**, 5325.
46 Y. Kim, N. Arumugam and J. B. Goodenough, *Chem. Mater.*, 2008, **20**, 470.
47 E. Gregoryanz, L. F. Lundegaard, M. I. McMahon, C. Guillaume, R. J. Nelmes and M. Mezouar, *Science*, 2008, **320**, 1054.
48 L. Wang, Z. Tang, B. Lorenz and A. M. Guloy, *J. Am. Ceram. Soc.*, 2008, **130**, 11258.
49 M. Imai, A. Sato, T. Aoyagi, T. Kimura, Y. Matsushita and N. Tsujii, *J. Am. Chem. Soc.*, 2008, **130**, 2886.
50 J. Winterlik, G. H. Fecher, C. Felser, M. Jourdan, K. Grube, F. Hardy, H. von Lohneysen, K. L. Holman and R. J. Cava, *Phys. Rev. B*, 2008, 78.
51 A. Tenga, S. Lidin, J. P. Belieres, N. Newman, Y. Wu and U. Haussermann, *J. Am. Chem. Soc.*, 2008, **130**, 15564.
52 S. H. Kim, M. Bostrom and D. K. Seo, *J. Am. Chem. Soc.*, 2008, **130**, 1384.

This journal is © The Royal Society of Chemistry 2009